

# Measurement of the fluorine atom concentration in a carbon tetrafluoride and helium atmospheric-pressure plasma

X Yang, S E Babayan and R F Hicks

Chemical Engineering Department, University of California, Los Angeles, CA 90095, USA

E-mail: rhicks@ucla.edu

Received 18 November 2002, in final form 17 March 2003

Published 17 July 2003

Online at [stacks.iop.org/PSST/12/484](http://stacks.iop.org/PSST/12/484)

## Abstract

The fluorine atom concentration has been measured in the downstream region of a low-temperature, atmospheric-pressure plasma fed with 739.0 Torr helium and 12.6 Torr carbon tetrafluoride ( $3.1 \times 10^{17} \text{ cm}^{-3}$ ). The fluorine atoms were titrated with  $\text{H}_2$  molecules, and the HF reaction product was detected by infrared spectroscopy. The radio-frequency gas discharge produced  $1.2 \times 10^{15} \text{ cm}^{-3}$  of F atoms, which was about two orders of magnitude higher than that found in low-pressure plasmas. The average electron density and temperature in the plasma was estimated to be  $6.1 \times 10^{11} \text{ cm}^{-3}$  and 2.5 eV, respectively. A numerical model of the plasma indicated that most of the fluorine atoms were generated by the reaction of  $\text{CF}_4$  with metastable helium atoms.

## 1. Introduction

Fluorine-containing plasmas are used extensively in the fabrication of microelectronic devices [1]. Reactive-ion etching of silicon dioxide with F atoms generated in low-pressure discharges is a key step in defining the submicron features found in very large scale integrated circuits [2, 3]. In this process, the fluorine provides chemical activity to the process, while ion bombardment ensures that anisotropic etching is achieved. Fluorocarbon-based plasmas also have been used to etch tungsten [4], remove damage from silicon wafers following chemical mechanical polishing [5], and isotropically etch MEMS devices [6]. Moreover, these discharges are of interest for decontaminating nuclear wastes, since F atoms have been found to strip away uranium and plutonium films [7, 8].

The chemistry and physics of low-pressure, carbon tetrafluoride plasmas has been the subject of much investigation [2]. One of the main objectives of this work was to determine the concentration of neutral fluorine atoms, since these species play a key role in the etching process. Fluorine atom concentrations have been measured by actinometry [9], vacuum ultraviolet absorption spectroscopy [10], appearance potential mass spectrometry [11], chemiluminescent titration [12], and mass spectrometric titration [13]. The titration techniques utilize the fast reactions of F with  $\text{Cl}_2$  or  $\text{H}_2$ . It has

been found that in weakly ionized plasmas containing pure  $\text{CF}_4$  at pressures between 0.01 and 1.0 Torr, the concentration of F atoms ranges from  $10^{11}$  to  $10^{13} \text{ cm}^{-3}$ .

Recently, atmospheric pressure, fluorocarbon-based plasmas have been examined for isotropic etching applications [5, 14]. One of the advantages of these systems is that they do not require insertion of the substrate into a vacuum chamber. Hicks and co-workers [15–19] have shown that stable, capacitive discharges may be produced at atmospheric pressure by feeding helium between two electrodes driven with radio-frequency (RF) power (e.g. 13.56 MHz). This discharge differs from other atmospheric-pressure plasmas, such as torches, dielectric barrier discharges, coronas, and cold cathodes, in that the neutral gas temperature is below 423 K and the weakly ionized gas is for the most part homogeneous in space and time [15]. Feeding  $\text{CF}_4$  to this plasma produces a reactive gas stream that etches tantalum at rates up to  $6.0 \mu\text{m min}^{-1}$  at a sample temperature of 573 K [19].

In this paper, we report on the measurement of the fluorine atom concentration in the afterglow of an atmospheric pressure, carbon tetrafluoride and helium plasma. The F atoms were detected by titrating the gas with  $\text{H}_2$ , and then recording the vibrational spectrum of the resultant HF molecules. We have found that the atmospheric-pressure plasma generates a large concentration of fluorine atoms downstream of the electrodes, in the range of  $10^{15} \text{ cm}^{-3}$ .

## 2. Experimental methods

The apparatus used in these experiments has been described previously [16]. A schematic of the source is shown in figure 1. It consisted of two parallel electrodes made of aluminium and separated by a gap 1.6 mm across. The upper electrode was  $2.2\text{ cm} \times 10.2\text{ cm}$ , and was connected to an RF power supply (13.56 MHz). An aluminium plate,  $10.2\text{ cm} \times 10.2\text{ cm}$ , was placed downstream of the upper electrode. The lower electrode, measuring  $10.2\text{ cm}$  in width and  $16.4\text{ cm}$  in length, was grounded and cooled with water. These parts were assembled together to provide a uniform duct  $1.6\text{ mm}$  in height throughout the length of the device. The sides of the gap parallel to the flow direction were sealed with barium fluoride windows so that infrared spectra of the gas could be recorded.

A tuned impedance probe (Advanced Energy RFZ 60) was used to measure the r.m.s. values of the discharge voltage and the RF current along with the coupled power to the plasma. The gas discharge was operated at  $84\text{ W cm}^{-3}$  of 13.56 MHz RF power, a total flow rate of  $65.6\text{ litre min}^{-1}$ , 739.0 Torr of helium and 12.6 Torr of carbon tetrafluoride. The flow rate produced a linear velocity of  $8.5\text{ m s}^{-1}$  (at 751.6 Torr and 373 K). The

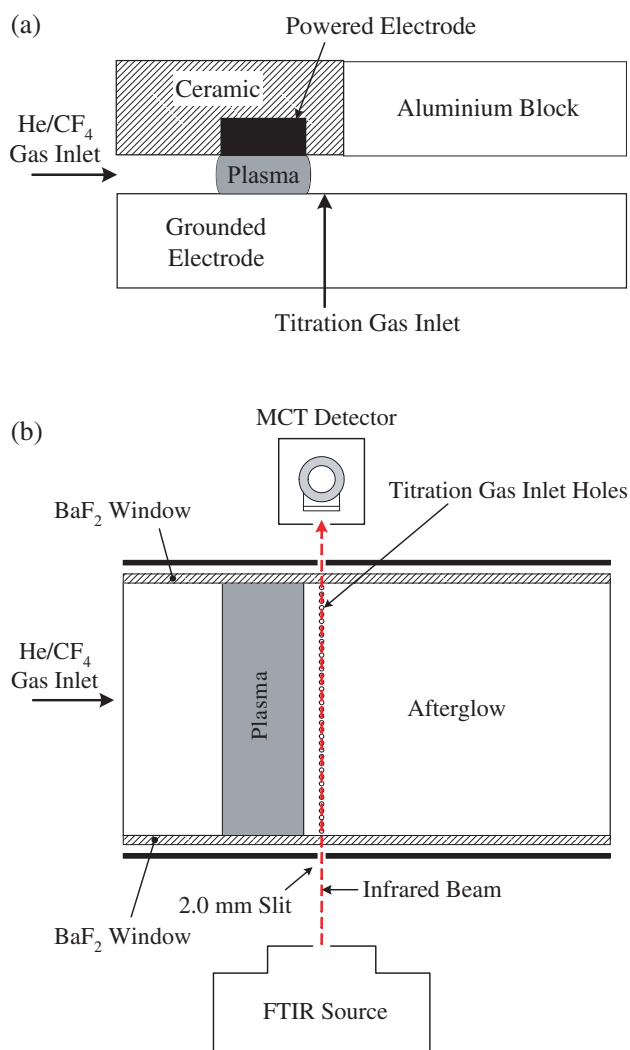


**Figure 1.** (a) Side view of the plasma source. (b) Top view of the interior of the plasma source.

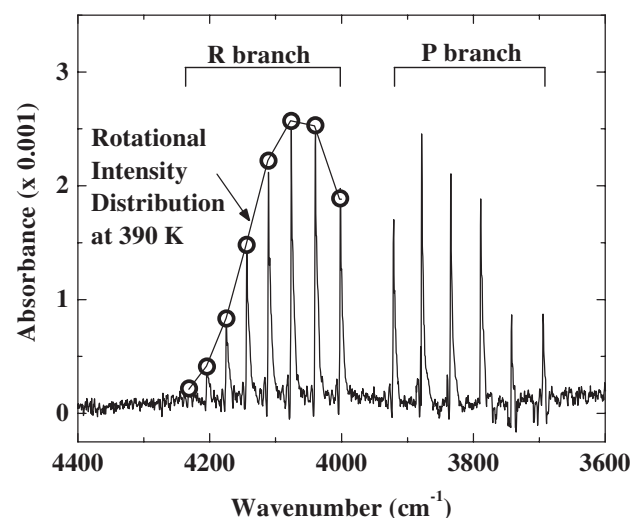
corresponding Reynolds number was 114, which was well within the laminar-flow regime. The helium and hydrogen were both of ultra-high purity (99.999%), while the carbon tetrafluoride was of semiconductor purity (99.95%).

For the titration experiments, an  $\text{H}_2$  and He mixture was fed to the system through a linear array of 50 holes, each  $0.8\text{ mm}$  in diameter. This array was located  $3\text{ mm}$  downstream of the edge of the plasma discharge, across the width of the lower grounded electrode. A Fourier-transform infrared spectrometer (BioRad FTS-7) was used to monitor the titration process. The infrared beam from the spectrometer passed through the gap between the two plates at the point where the hydrogen and plasma effluent mixed. Slits on each side of the  $\text{BaF}_2$  windows restricted the beam width to  $2\text{ mm}$ . The infrared light was collected with a mercury-cadmium-telluride (MCT) detector at a resolution of  $1\text{ cm}^{-1}$  and by signal averaging 256 scans.

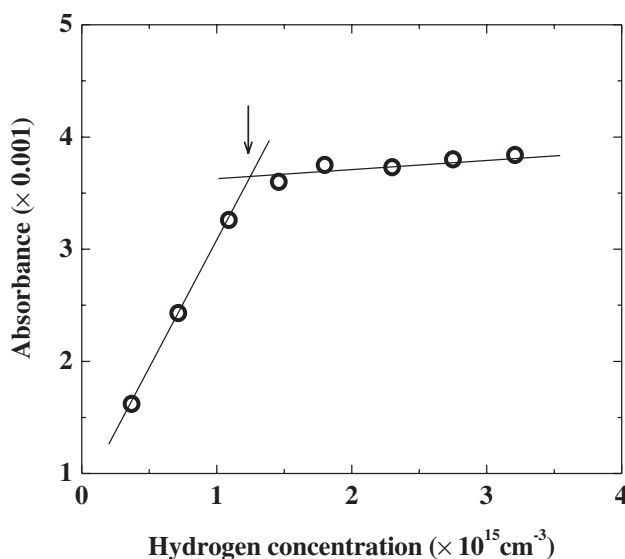
## 3. Results and discussion

Figure 2 shows the infrared spectrum of hydrogen fluoride obtained by adding  $0.7 \times 10^{15}\text{ cm}^{-3}$  hydrogen to the afterglow of the  $\text{CF}_4$  and He plasma. The rotational structure associated with the P and R branches of the vibrational spectrum is clearly observed. We have used one of the peaks in the R branch to monitor the amount of HF produced in the titration experiments. In the figure, the curve connecting the peaks in the R branch is the rotational intensity distribution calculated from HITRAN data [20] for a gas temperature of 390 K. A thermocouple suspended in the gas at the titration point yielded a temperature of 373 K.

The dependence of the infrared peak height of hydrogen fluoride (at  $4039.7\text{ cm}^{-1}$ ) on the hydrogen concentration in the gas downstream of the plasma is shown in figure 3. The peak intensity increases linearly with the hydrogen concentration up to about  $1.0 \times 10^{15}\text{ cm}^{-3}$ , and thereafter remains relatively constant. A plateau is observed at the point where the F atom concentration begins to limit the rate of production of hydrogen fluoride. Since the reaction stoichiometry is 1 : 1,



**Figure 2.** Infrared absorption spectrum of HF taken during the titration of F atoms with  $\text{H}_2$  in the  $\text{CF}_4$ -He plasma afterglow.



**Figure 3.** The dependence of the intensity of the HF absorption peak at  $4039.7 \text{ cm}^{-1}$  on the  $\text{H}_2$  concentration in the plasma afterglow. The arrow denotes the titration point.

the knee in the curve corresponds to a hydrogen concentration that equals the F atom concentration:  $[\text{F}] = [\text{H}_2]$  (at knee) =  $1.2 \times 10^{15} \text{ cm}^{-3}$ . Given the uncertainties inherent in this method, we estimate that this measurement is accurate to within  $\pm 20\%$  of the value.

For the titration technique to work, the consumption rate of  $\text{H}_2$  by F has to exceed the consumption rates of  $\text{H}_2$  by other reactions. This is indeed the case here, given that the bimolecular rate constant for this reaction is  $4.4 \times 10^{-11} \text{ cm}^3 \text{ s}^{-1}$  at 390 K [21]. The next fastest reaction involving fluorine atoms is three-body recombination,  $\text{F} + \text{F} + \text{He} \rightarrow \text{F}_2 + \text{He}$ , which has a pseudo-bimolecular rate constant of  $4.8 \times 10^{-14} \text{ cm}^3 \text{ s}^{-1}$  at 390 K [22]. The reactions of  $\text{CF}_x$  radicals with F or  $\text{H}_2$  are not significant, given that the radical concentrations are several orders of magnitude lower than the F and  $\text{H}_2$  concentrations at the titration point (see later). It should be noted that the F atom density is in the same range as the O and N atom densities obtained by feeding either  $\text{O}_2$  or  $\text{N}_2$  to the helium-stabilized atmospheric-pressure plasma [16, 17].

A one-dimensional ‘plug-flow’ model has been developed to determine the concentration of the fluorine atoms and other reactive species as they evolve in time or distance downstream of the reactor. This model assumes that there is no gas mixing in the axial flow direction and perfect mixing in the cross-stream direction. In addition, the temperature is assumed to be constant, equal to 390 K. The reaction mechanism is given in table 1. It includes elementary reactions among neutral species (He,  $\text{CF}_4$ , F,  $\text{CF}_3$ ,  $\text{CF}_2$ , CF,  $\text{C}_2\text{F}_6$ ,  $\text{C}_2\text{F}_5$ ,  $\text{C}_2\text{F}_4$ ,  $\text{C}_2\text{F}_3$ , and  $\text{F}_2$ ), ions ( $\text{F}^-$ ,  $\text{CF}_3^-$ ,  $\text{CF}_3^+$ ,  $\text{CF}_2^+$ ,  $\text{He}^+$ , and  $\text{He}_2^+$ ), and electronically excited helium ( $\text{He}^*$  and  $\text{He}_2^*$ ). The numerical model consists of the simultaneous set of material balances for these 19 species.

In order to calculate the rate constants for electron-neutral reactions given in table 1, we needed an estimate of the average electron density and temperature in the plasma. These parameters were estimated for the plasma, based on

the measured r.m.s. current and discharge voltage, and using the zero-dimensional power balance reported by Park *et al* [18, 24]. An estimate of the electron density,  $n_e$ , can be obtained from the relationship between the RF current density,  $J$ , and the electric field strength,  $E$ :

$$J = -n_e e \mu_e E \quad (1)$$

where  $e$  is a unit of electric charge, and  $\mu_e$  is the electron mobility ( $\text{cm}^2 \text{ V}^{-1} \text{ s}^{-1}$ ). Knowing the plasma density, the average electron temperature,  $T_e$ , can be calculated from a zero-dimensional power balance on the plasma:

$$P_{\text{in}} \approx n_e \left( \frac{3}{2} k T_e - \frac{3}{2} k T_n \right) 2 \frac{m_e}{m_{\text{He}}} \nu_{\text{en}} \quad (2)$$

Here,  $P_{\text{in}}$  is the input power density ( $\text{W cm}^{-3}$ ),  $T_n$  is the gas temperature (eV),  $m_e/m_{\text{He}}$  is the mass ratio between the electron and the helium atom, and  $\nu_{\text{en}}$  is the collision frequency (Hz) for elastic scattering of electrons with helium. This equation assumes that the plasma power is dissipated primarily through elastic collisions of electrons with neutrals.

The r.m.s. current and voltage measured for the  $\text{CF}_4$ -He discharge were 8.03 A and 337 V, respectively, which corresponds to a current density,  $J$ , of  $0.35 \text{ A cm}^{-2}$  and an electric field,  $E$ , of  $2106 \text{ V cm}^{-1}$ . From equations (1) and (2), an electron density and temperature of  $6.1 \times 10^{11} \text{ cm}^{-3}$  and 2.5 eV, respectively, were obtained.

The kinetics of the helium reactions, R1–R9, was taken from a theoretical study of the atmospheric pressure helium discharge conducted by Yuan and Raja [26]. The rate coefficients for electron-impact dissociation and electron-attachment dissociation, R16–R23, were computed using the cross sections,  $Q_d(\varepsilon)$ , reported in the literature [28–30] and the electron energy distribution,  $f(\varepsilon)$ :

$$k_d = \int_0^\infty \left( \frac{2\varepsilon}{m_e} \right)^{1/2} Q_d(\varepsilon) f(\varepsilon) d\varepsilon \quad (3)$$

where  $\varepsilon$  is the electron energy. A Maxwellian distribution with a mean electron energy of 2.5 eV has been assumed here. This is a close estimation to the electron energy distribution in the atmospheric-pressure plasma because the electrical field strength/pressure ratio ( $E/p$ ) is low and the plasma is highly collisional. The rate constants for the radical reactions have been evaluated at atmospheric pressure and are well established [22, 23, 25].

In the simulations, reactions R1–R39 are employed inside the plasma, while downstream of the discharge, only reactions involving neutral species are used. At atmospheric pressure, the electrons are extinguished within a few hundred micrometres after leaving the gas space between the electrodes [15].

The predicted densities of the ions and excited helium species in the discharge are shown in figure 4. The gas feed is the same as in the experiments: 12.6 Torr  $\text{CF}_4$  and 739.0 Torr helium. The steady state densities of ions,  $\text{He}^*$  and  $\text{He}_2^*$  are achieved within 1.0 mm of the leading edge of the plasma. Note that the density of  $\text{He}^*$  is about 100 times higher than that of  $\text{He}_2^*$ . The most abundant ions are  $\text{CF}_3^+$ ,  $\text{F}^-$ , and  $\text{CF}_3^-$ , which are in the range of  $10^{12}$ – $10^{13} \text{ cm}^{-3}$ . The total

**Table 1.** Reaction mechanism for the CF<sub>4</sub>-He atmospheric-pressure plasma.

Reactions	Rate constants <sup>a</sup>	Ref.
R1 e + He → He <sup>+</sup> + 2e	$2.584 \times 10^{-12} T_e^{0.68} \exp(-24.6/T_e)$	[26]
R2 e + He → He* + e	$2.308 \times 10^{-10} T_e^{0.31} \exp(-19.8/T_e)$	[26]
R3 e + He* → He + e	$1.099 \times 10^{-11} T_e^{0.31}$	[26]
R4 e + He <sub>2</sub> * → He <sub>2</sub> <sup>+</sup> + 2e	$1.268 \times 10^{-12} T_e^{0.71} \exp(-3.4/T_e)$	[26]
R5 e + He* → He <sup>+</sup> + 2e	$4.661 \times 10^{-10} T_e^{0.6} \exp(-4.78/T_e)$	[26]
R6 e + He <sub>2</sub> <sup>+</sup> → He* + He	$5.386 \times 10^{-7} T_e^{-0.5}$	[26]
R7 He <sup>+</sup> + He + He → He <sub>2</sub> <sup>+</sup> + He	$2.0 \times 10^{-31}$	[26]
R8 He* + He* → He <sup>+</sup> + He + e	$2.7 \times 10^{-10}$	[26]
R9 He* + He + He → He <sub>2</sub> * + He	$1.3 \times 10^{-33}$	[26]
R10 He* + CF <sub>4</sub> → CF <sub>3</sub> <sup>+</sup> + F + He + e	$1.8 \times 10^{-10}$	[27]
R11 He <sub>2</sub> * + CF <sub>4</sub> → CF <sub>3</sub> <sup>+</sup> + F + 2He + e	$1.8 \times 10^{-10}$	[27]
R12 He <sup>+</sup> + CF <sub>4</sub> → CF <sub>3</sub> <sup>+</sup> + F + He	$2.7 \times 10^{-10}$	[27]
R13 He <sup>+</sup> + CF <sub>4</sub> → CF <sub>2</sub> <sup>+</sup> + 2F + He	$2.7 \times 10^{-10}$	[27]
R14 He <sub>2</sub> <sup>+</sup> + CF <sub>4</sub> → CF <sub>3</sub> <sup>+</sup> + F + 2He	$2.7 \times 10^{-10}$	[27]
R15 He <sub>2</sub> <sup>+</sup> + CF <sub>4</sub> → CF <sub>2</sub> <sup>+</sup> + 2F + 2He	$2.7 \times 10^{-10}$	[27]
R16 e + CF <sub>4</sub> → CF <sub>3</sub> + F <sup>-</sup>	$4.7 \times 10^{-12}$	[28]
R17 e + CF <sub>4</sub> → CF <sub>3</sub> <sup>-</sup> + F	$1.6 \times 10^{-12}$	[28]
R18 CF <sub>4</sub> + e → CF <sub>3</sub> + F + e	$3.6 \times 10^{-12}$	[29]
R19 CF <sub>4</sub> + e → CF <sub>2</sub> + 2F + e	$6.3 \times 10^{-13}$	[29]
R20 CF <sub>3</sub> + e → CF <sub>2</sub> + F + e	$3.6 \times 10^{-12}$	[29] <sup>b</sup>
R21 CF <sub>2</sub> + e → CF + F + e	$3.6 \times 10^{-12}$	[29] <sup>b</sup>
R22 C <sub>2</sub> F <sub>6</sub> + e → CF <sub>3</sub> + CF <sub>3</sub> + e	$3.6 \times 10^{-11}$	[30]
R23 C <sub>2</sub> F <sub>4</sub> + e → CF <sub>2</sub> + CF <sub>2</sub> + e	$3.6 \times 10^{-11}$	[30] <sup>c</sup>
R24 F <sup>-</sup> + CF <sub>3</sub> <sup>+</sup> → F + CF <sub>3</sub>	$1.0 \times 10^{-7}$	[31]
R25 F <sup>-</sup> + CF <sub>2</sub> <sup>+</sup> → F + CF <sub>2</sub>	$1.0 \times 10^{-7}$	[31]
R26 CF <sub>3</sub> <sup>-</sup> + CF <sub>3</sub> <sup>+</sup> → CF <sub>3</sub> + CF <sub>3</sub>	$1.0 \times 10^{-7}$	[31]
R27 CF <sub>3</sub> + F + M → CF <sub>4</sub> + M	$9.6 \times 10^{-31}$	[23]
R28 CF <sub>2</sub> + F + M → CF <sub>3</sub> + M	$5.3 \times 10^{-31}$	[23]
R29 CF + F + M → CF <sub>2</sub> + M	$1.4 \times 10^{-31}$	[23]
R30 CF <sub>3</sub> + CF <sub>3</sub> + M → C <sub>2</sub> F <sub>6</sub> + M	$4.1 \times 10^{-31}$	[23]
R31 CF <sub>2</sub> + CF <sub>2</sub> + M → C <sub>2</sub> F <sub>4</sub> + M	$2.5 \times 10^{-33}$	[23]
R32 CF <sub>2</sub> + CF <sub>3</sub> + M → C <sub>2</sub> F <sub>5</sub> + M	$4.9 \times 10^{-32}$	[23]
R33 F + C <sub>2</sub> F <sub>4</sub> → CF <sub>3</sub> + CF <sub>2</sub>	$4.0 \times 10^{-11}$	[23]
R34 F + C <sub>2</sub> F <sub>5</sub> → CF <sub>3</sub> + CF <sub>3</sub>	$1.0 \times 10^{-11}$	[23]
R35 CF + CF <sub>2</sub> + M → C <sub>2</sub> F <sub>3</sub> + M	$5.1 \times 10^{-32}$	[23]
R36 F + C <sub>2</sub> F <sub>3</sub> + M → C <sub>2</sub> F <sub>4</sub> + M	$5.1 \times 10^{-32}$	[23]
R37 F + F + M → F <sub>2</sub> + M	$2.4 \times 10^{-33}$	[22]
R38 F <sub>2</sub> + CF <sub>2</sub> → CF <sub>3</sub> + F	$4.6 \times 10^{-13}$	[25]
R39 F <sub>2</sub> + CF <sub>3</sub> → CF <sub>4</sub> + F	$1.9 \times 10^{-14}$	[25]

<sup>a</sup> Rate constants have units of cm<sup>3</sup> s<sup>-1</sup> and cm<sup>6</sup> s<sup>-1</sup> for two- and three-body collisions, respectively.

<sup>b</sup> Estimated by analogy to R18.

<sup>c</sup> Estimated by analogy to R22.

charge summed over all these ions and electrons equals zero, confirming that the plasma is neutral. It is further noted that the F<sup>-</sup> concentration is  $3.0 \times 10^{12}$  cm<sup>-3</sup>, or about five times higher than the electron density. This indicates that the plasma is ‘electronegative,’ which is consistent with other studies of gas discharges containing fluorocarbons [27].

The predicted profiles of the neutral species in the plasma and in the afterglow downstream of the electrodes are shown in figure 5. The profile for carbon tetrafluoride is not shown in the figure. Its density is  $3.1 \times 10^{17}$  cm<sup>-3</sup>. The CF<sub>4</sub> is dissociated in the plasma into F, CF<sub>2</sub>, and CF<sub>3</sub>. The CF<sub>2</sub> and CF<sub>3</sub> achieve concentrations in the range of  $10^{13}$  and  $10^{14}$  cm<sup>-3</sup> inside the discharge, but are rapidly converted to C<sub>2</sub>F<sub>6</sub> in the afterglow. In contrast, the concentration of F atoms rises to  $1.3 \times 10^{15}$  cm<sup>-3</sup> inside the plasma, and decreases only slightly to  $1.0 \times 10^{15}$  cm<sup>-3</sup> over the 20 mm length of the afterglow region. The F atoms are stable downstream of the discharge because they are consumed by three-body collisions, which are

infrequent at these conditions. The F atom density predicted by the numerical simulation is in good agreement with the value measured by H<sub>2</sub> titration (see figure 3). This suggests that the numerical model captures the physics and chemistry of the process.

The fluorine atoms are produced by several elementary processes in the discharge, involving collisions of CF<sub>4</sub> with energetic helium species and electrons. By running several simulations, it was determined that reactions R10 and R16–R18 are kinetically significant. In particular, the reaction of CF<sub>4</sub> with metastable helium, R10, accounts for 70% of the fluorine atoms generated in the plasma.

#### 4. Conclusions

In summary, the fluorine atom concentration produced by the dissociation of carbon tetrafluoride in a helium-stabilized, atmospheric-pressure plasma has been measured for the first

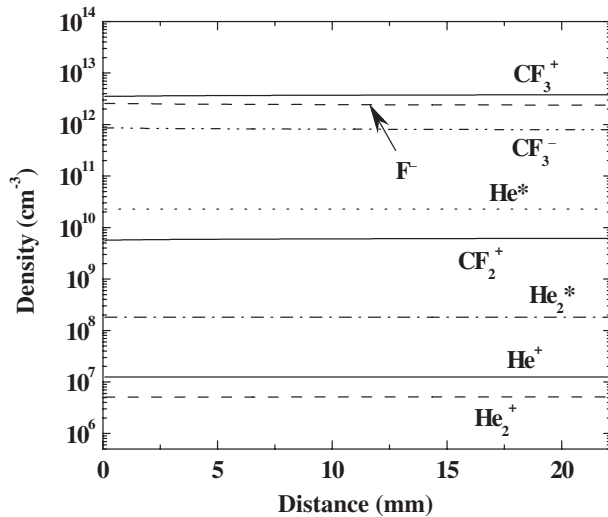


**Figure 4.** The predicted densities of the ions and excited helium species in the  $\text{CF}_4$  and He atmospheric-pressure plasma.

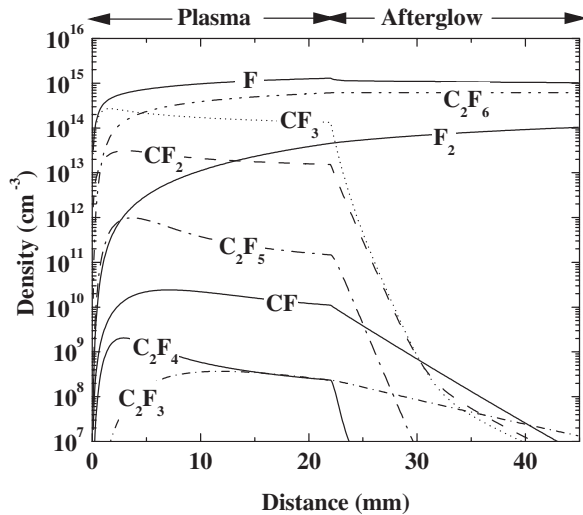


**Figure 5.** The predicted profiles of the neutral species in the  $\text{CF}_4$  and He atmospheric-pressure plasma and afterglow regions.

time. The F atom density 3 mm downstream of the electrodes is  $1.2 \times 10^{15} \text{ cm}^{-3}$  at 84 W  $\text{cm}^{-3}$ , 12.6 Torr  $\text{CF}_4$ , and 739.0 Torr helium. This concentration is several orders of magnitude higher than that recorded in low-pressure  $\text{CF}_4$  discharges.

### Acknowledgments

This research was supported by the US Department of Energy, Environmental Management Sciences Program (Grant No FG07-00ER45857).

### References

- [1] Wolf S 1990 *Silicon Processing for the VLSI Era* vol 2 (Sunset Beach, CA: Lattice Press)
- [2] Lieberman M A and Lichtenberg A J 1994 *Principles of Plasma Discharges and Materials Processing* (New York: Wiley)
- [3] Nojiri K and Iguchi E 1995 *J. Vac. Sci. Technol. B* **13** 1451
- [4] Bestwick T D and Oehrlein G S 1989 *J. Appl. Phys.* **66** 5034
- [5] Savastouk S, Siniaguine O and Hammond M L 1998 *Solid State Technol.* **41** 133
- [6] Das N C 2002 *Solid-State Electron.* **46** 501
- [7] Martz J C, Hess D W, Haschke J M, Ward J W and Flamm B F 1991 *J. Nucl. Mater.* **182** 277
- [8] Kim Y S, Min J Y, Bae K K and Yang M S 1999 *J. Nucl. Mater.* **270** 253
- [9] Jenq J S, Ding J, Taylor J W and Hershkovitz N 1994 *Plasma Sources Sci. Technol.* **3** 154
- [10] Sasaki K, Kawai Y, Suzuki C and Kadota K 1997 *J. Appl. Phys.* **82** 5938
- [11] Tserapi A, Schwarzenbach W, Derouard J and Sadeghi N 1997 *J. Vac. Sci. Technol. A* **15** 3120
- [12] Mogab C J, Adams A C and Flamm D L 1978 *J. Appl. Phys.* **49** 3796
- [13] Suzuki K, Ninomiya K and Nishimatsu S 1984 *Vacuum* **34** 953
- [14] Kataoka Y, Kanoh M, Makino N, Suzuki K, Saitoh S, Miyajima H and Mori Y 2000 *Japan. J. Appl. Phys.* **39** 294
- [15] Schütze A, Jeong J Y, Babayan S E, Park J, Selwyn G S and Hicks R F 1998 *IEEE Trans. Plasma Sci.* **26** 1685
- [16] Jeong J Y, Park J, Henins I, Babayan S E, Tu V J, Selwyn G S, Ding G and Hicks R F 2000 *J. Phys. Chem.* **104** 8027
- [17] Babayan S E, Ding G and Hicks R F 2001 *Plasma Chem. Plasma Process.* **21** 505
- [18] Park J, Henins I, Herrmann H W, Selwyn G S and Hicks R F 2001 *J. Appl. Phys.* **89** 20
- [19] Tu V J, Jeong J Y, Schütze A, Babayan S E, Ding G, Selwyn G S and Hicks R F 2000 *J. Vac. Sci. Technol. A* **18** 2799
- [20] Rothman L S 1998 *J. Quant. Spectrosc. Radiat. Transfer* **60** 665
- [21] Levitt B P 1973 *Physical Chemistry of Fast Reactions* vol 1 (New York: Plenum)
- [22] Duman E L, Tishchenko N P and Shmatov I P 1987 *Dokl. Phys. Chem.* **295** 5
- [23] Ryan K R and Plumb I C 1986 *Plasma Chem. Plasma Process.* **6** 205
- [24] Park J, Henins I, Herrmann H W and Selwyn G S 2000 *Phys. Plasmas* **7** 3141
- [25] Burgess D R F, Zachariah M R Jr, Tsang W and Westmoreland P R 1996 *Prog. Energy Combust. Sci.* **21** 453
- [26] Yuan X and Raja L L 2003 *IEEE Trans. Plasma Sci.* in press
- [27] Mutsukura N and Shimada M 1997 *J. Vac. Sci. Technol. A* **15** 1828
- [28] Christophorou L G, Olthoff J K and Rao M V V S 1996 *J. Phys. Chem. Ref. Data* **25** 1341
- [29] Sugai H, Toyoda H, Nakano T and Goto M 1995 *Contrib. Plasma Phys.* **35** 415
- [30] Hayashi M 1987 in *Gaseous Dielectrics* V ed L G Christophorou and D W Bouldin (New York: Pergamon)
- [31] Olson R E, Peterson J R and Moseley J 1971 *J. Chem. Phys.* **53** 3391